

1 Linking Increased Isotope Fractionation at Low Concentrations to 2 Enzyme Activity Regulation: 4-Cl Phenol Degradation by 3 *Arthrobacter chlorophenolicus* A6

4 Kankana Kundu,* Aileen Melsbach, Benjamin Heckel, Sarah Schneidemann, Dheeraj Kanapathi,
5 Sviatlana Marozava, Juliane Merl-Pham, and Martin Elsner*



Cite This: <https://doi.org/10.1021/acs.est.1c04939>



Read Online

ACCESS |



Metrics & More

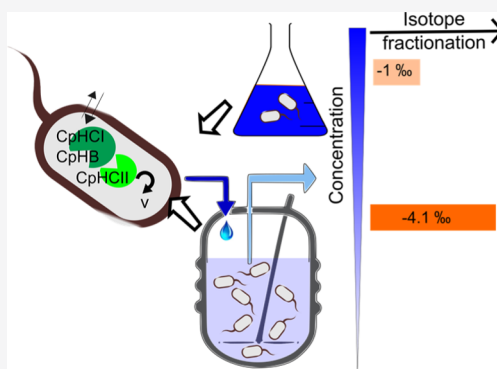


Article Recommendations



Supporting Information

6 **ABSTRACT:** Slow microbial degradation of organic trace chemicals (“micro-
7 pollutants”) has been attributed to either downregulation of enzymatic turnover
8 or rate-limiting substrate supply at low concentrations. In previous
9 biodegradation studies, a drastic decrease in isotope fractionation of atrazine
10 revealed a transition from rate-limiting enzyme turnover to membrane
11 permeation as a bottleneck when concentrations fell below the Monod constant
12 of microbial growth. With degradation of the pollutant 4-chlorophenol (4-CP)
13 by *Arthrobacter chlorophenolicus* A6, this study targeted a bacterium which adapts
14 its enzyme activity to concentrations. Unlike with atrazine degradation, isotope
15 fractionation of 4-CP increased at lower concentrations, from $\epsilon(C) = -1.0 \pm$
16 0.5% in chemostats ($D = 0.090 \text{ h}^{-1}$, 88 mg L^{-1}) and $\epsilon(C) = -2.1 \pm 0.5\%$ in
17 batch ($c_0 = 220 \text{ mg L}^{-1}$) to $\epsilon(C) = -4.1 \pm 0.2\%$ in chemostats at $90 \mu\text{g L}^{-1}$.
18 Surprisingly, fatty acid composition indicated increased cell wall permeability at
19 high concentrations, while proteomics revealed that catabolic enzymes (CpHCl
20 and CphCII) were differentially expressed at $D = 0.090 \text{ h}^{-1}$. These observations support regulation on the enzyme activity level—
21 through either a metabolic shift between catabolic pathways or decreased enzymatic turnover at low concentrations—and, hence,
22 reveal an alternative end-member scenario for bacterial adaptation at low concentrations. Including more degrader strains into this
23 multidisciplinary analytical approach offers the perspective to build a knowledge base on bottlenecks of bioremediation at low
24 concentrations that considers bacterial adaptation.



25 **KEYWORDS:** limits of biodegradation, mass transfer, enzyme regulation, cell wall permeability, chemostat, proteomics, isotope effect

26 ■ INTRODUCTION

27 Organic contaminants such as pesticides, personal care
28 products, steroid hormones, and pharmaceuticals are fre-
29 quently detected in the aquatic environment at low
30 concentrations (ng L^{-1} to $\mu\text{g L}^{-1}$).^{1,2} These low-level
31 contaminants—referred to as chemical micropollutants—bear
32 potential to impact ecosystems³ so that their natural
33 degradation is of great relevance. Many of these pollutants
34 were found to be biodegradable in studies at high
35 concentrations, at which degrading organisms could be
36 cultivated and isolated from contaminated environments.^{4–6}
37 Nonetheless, the increasingly frequent detection of micro-
38 pollutants in aquatic environments indicates that their turnover
39 must be very slow to nonexistent at low environmental
40 concentrations.^{7,8} This observation is mirrored by the
41 persistence of assimilable organic carbon (AOC) in aquatic
42 environments on the order of $1\text{--}100 \mu\text{g L}^{-1}$ where
43 concentrations of individual sugars are only a few $\mu\text{g L}^{-1}$.
44 This suggests that contaminants and degradable biomolecules
45 alike may become “persistent by dilution”.⁹ Despite such slow

46 degradation of AOC and despite an energy-limited environ-
47 ment, where microorganisms face continuous exposure to low
48 concentrations, viable cell counts still amount to 10^5 to 10^6
49 cells mL^{-1} ,^{9–11} of which most ($\sim 70\%$) maintain their
50 activity.^{12,13} Hence, understanding activity, intrinsic limita-
51 tions, and microbial adaptation to low concentrations is
52 important, not only to understand the physiology of micro-
53 organisms under extreme environmental conditions but also
54 for micropollutant management and remediation strategies
55 when compounds are in principle biodegradable and organisms
56 are active, but degradation is inexplicably slow.

57 Two competing paradigms may rationalize such a low
58 activity at low concentrations. First, uptake of micropollutants

Received: July 23, 2021

Revised: January 23, 2022

Accepted: January 26, 2022

59 into microbial cells (active/passive transport) may become
60 rate-limiting when the enzyme reaction shifts from zero- to
61 first-order kinetics at low concentrations so that intracellular
62 substrate levels are drained.^{14–16} Alternatively, enzymatic
63 turnover may become rate-limiting when microorganisms
64 adapt their physiology to low concentrations—for example,
65 by switching to maintenance mode and downregulating
66 catabolic enzymes^{17,18}—so that enzymatic degradation slows
67 or even stalls below a particular low concentration. With
68 conventional methods, it is challenging to identify the
69 bottleneck—mass transfer or enzyme activity—under these
70 circumstances. Insights from compound-specific isotope
71 analysis (CSIA) offer complementary evidence. CSIA measures
72 the ratios of stable isotopes at their natural abundance in a
73 compound. The isotope effect of enzymatic reactions usually
74 discriminates against heavy isotopes and, therefore, leads to an
75 enrichment of heavy relative to light isotopes in the remaining
76 pollutant molecules next to the enzyme.¹⁹ If this enrichment
77 can also be observed outside the cell in solution, it makes CSIA
78 a unique approach to determine turnover of micropollutants in
79 natural systems. Such an isotope fractionation is typically
80 observed in microbial degradation at high concentrations when
81 enzymes inside the cell are substrate-saturated and enzymatic
82 turnover runs at zero-order kinetics (V_{\max}). Under these
83 conditions, mass transfer across the cell membrane is fast in
84 comparison, and intra- and extracellular substrate concen-
85 trations are in rapid equilibrium.^{20,21} At low concentrations—
86 depending upon microbial adaptation—however, two scenar-
87 ios can arise: one where the enzyme reaction remains the rate-
88 determining step and the other where mass transfer into the
89 cell becomes limiting.²¹ In analogy to insights from isotope
90 fractionation of CO₂ in photosynthesis of C₃ versus C₄ plants²²
91 or in algae when uptake becomes limiting,^{23,24} here, observable
92 isotope fractionation can provide conclusive evidence. (i) If
93 intracellular concentrations fall below the Michaelis-Menten
94 constant, enzymatic turnover will no longer run at saturation
95 but follow first-order kinetics. The enzyme reaction may
96 consequently become fast relative to mass transfer into and out
97 of the cell so that cell membrane passage becomes the
98 bottleneck of the overall transformation (Scenario 1 above). In
99 such a situation, the isotope effect—which still occurs next to
100 the enzyme—will no longer be represented outside the cell
101 because molecules are quicker to be converted than to diffuse
102 out and make the isotope discrimination visible in solution.
103 Hence, concomitant to mass transfer limitations, the isotope
104 fractionation that is experimentally observed outside the cell
105 will become masked and decrease.^{15,16,25} (ii) In contrast, if the
106 enzymatic turnover remains slower than the mass transfer
107 across the cell membrane—corresponding to scenario 2
108 mentioned above—the opposite trend will be observed:
109 isotope fractionation will be fully expressed, similarly as at
110 high concentrations.

111 In degradation of the prevalent micropollutant atrazine with
112 *Arthrobacter aureus* TC1,²⁶ a drastic decrease in isotope
113 fractionation revealed that scenario 1 prevailed: at about 60 μg
114 L⁻¹, mass transfer through the cell membrane became limiting
115 implying that the enzyme machinery remained fully active at
116 low concentrations.^{27,28} While intriguing, insights from this
117 study are based on the response of only one microorganism
118 cultivated with one specific micropollutant, and it represents a
119 case where enzyme activity was not reported to respond to
120 specific micropollutant concentrations. It is well-recognized
121 that organisms exist (i) whose enzyme activity is regulated by

the micropollutant concentration, either on the expression
level of metabolic pathways (up/downregulation^{9,18,29,30}) or
directly on the level of enzyme activity (inhibition^{31–33} and
activation^{34,35}), and, further, (ii) whose cell membrane may
change in response to high versus low concentrations of a
compound so that membrane permeability and, thus, mass
transfer are also modulated.^{36,37}

Phenolic compounds, for example, 4-chlorophenol (4-CP),
represent a specific category of pollutants which are known for
acute toxicity that has a regulating effect on both enzyme
activity^{38,39} and cell membrane fluidity so that mass transfer
across the cell membrane is also modulated.⁴⁰ Attention has
been paid to isolation of degrader strains and to the influence
of high, toxic concentrations on growth kinetics.^{5,41} In
contrast, it remains to be investigated how degraders adapt
to low concentrations and what influence changes in cell
membrane fluidity, as well as enzyme activity regulation, have
on limiting 4-CP turnover at low concentrations. Specifically, it
was our objective to investigate whether concentrations may
have a regulating effect on enzymatic turnover of 4-CP so
that—unlike in the case of *A. aureus* TC1—it would be
enzymatic turnover rather than mass transfer through the cell
membrane that becomes rate-limiting at low concentrations.
To explore this, *Arthrobacter chlorophenolicus* A6 was chosen as
a model microorganism which can degrade various phenolic
compounds.⁵ The availability of a fully sequenced genome,⁴²
experimental evidence of membrane adaptation at varying
concentrations,³⁷ and the presence of inducible degradation
enzymes that can catalyze two catabolic pathways simulta-
neously^{42,43} make this organism a promising candidate to
explore the effect of physiological adaptation/regulation on the
bottleneck of phenolic compound degradation at low
concentrations. Previous studies targeted CSIA during
biodegradation of phenolic compounds at high concentra-
tions⁴⁴ or they explored the indirect influence of phenolic
compounds on isotope fractionation of a different substrate—
the electron acceptor nitrate.⁴⁵ Here, it was our aim to directly
measure the observable isotope fractionation of 4-CP during
ongoing degradation along with analysis of membrane fatty
acids and the proteome state of the cells at varying
concentrations. To investigate two end-member scenarios, *A.*
chlorophenolicus A6 was cultivated at high concentrations (mg
L⁻¹) in batch and chemostats and at low concentrations (μg
L⁻¹) in chemostats. In both cases, observable isotope
fractionation was measured to explore limitations by mass
transfer. To probe for physiological adaptation, (i) flow
cytometry was performed to inform about the fraction of
viable to total cells, (ii) comparative label-free proteomics was
conducted to observe changes in protein expression, and (iii)
the cell membrane fatty acid composition was analyzed to test
for changes in membrane fluidity.

■ MATERIALS AND METHODS

Cultivation in Batch and Chemostats. *A. chloropheno-*
licus A6 (DSMZ, Germany) was grown on mineral salt (MS)
medium supplemented with 220 (1.71 mM) mg L⁻¹ 4-CP and
0.5 g L⁻¹ (6.25 mM) NH₄NO₃ (Sigma-Aldrich, Germany) as a
source of C and N, respectively.⁵ The medium was prepared in
MilliQ water where the total organic carbon content was less
than 10 μg L⁻¹ and the pH was adjusted to 7.2 with sodium
hydroxide (1.0 M). The medium was autoclaved at 121 °C for
20 min and cooled. After autoclaving, the media was spiked
with 4-CP (≥99%, 1.3 g mL⁻¹, Sigma-Aldrich, Germany) and

184 NH_4NO_3 (stock solution = 20 g L^{-1} and filter-sterilized) to
185 reach a final concentration of 220 mg L^{-1} and 0.5 g L^{-1} ,
186 respectively. This was followed by the addition of a filter-
187 sterilized $\text{FeCl}_3 \cdot 6\text{H}_2\text{O}$ solution (5.14 mg L^{-1}). To prepare a
188 preculture for subsequent batch and chemostats (continuous
189 cultivation) degradation experiments, *A. chlorophenolicus* A6
190 was grown on MS media with 4-CP and NH_4NO_3 in a shaken
191 flask at 300 rpm until an optical density at 600 nm (OD_{600}) of
192 0.15 (mid-exponential phase) was reached. For batch
193 degradation experiments, cells were harvested by centrifuging
194 50 mL of preculture, washing the pellet twice in sterile MS
195 media, and resuspending it in 1 mL of sterile MS media. This
196 suspension was added to 500 mL of MS media supplemented
197 with 220 mg L^{-1} 4-CP to initiate the degradation of 4-CP at 25
198 $^\circ\text{C}$. Subsequently, samples were taken for concentration and
199 isotope analysis of 4-CP and cell concentration measurements
200 over time and data were used to estimate Haldane inhibition
201 kinetic constants (see the Supporting Information).

202 The continuous cultivation of *A. chlorophenolicus* A6 was
203 performed in custom-made bioreactors equipped with a
204 magnetic stirrer, where the agitation speed was maintained at
205 300 rpm (Supporting Information, Figure S1). In such
206 chemostats, the growth of microorganisms is determined by
207 the rate of in- and outflow, where wash-out of media and
208 microorganisms is balanced by continuous addition of media
209 and growth of bacteria. At high flow/dilution rates D [defined
210 as the ratio of the medium flow rate (mL h^{-1}) and cultivation
211 volume (L)], the reactor volume is quickly exchanged so that
212 bacteria grow more quickly to maintain a steady-state cell
213 concentration. At low D , in contrast, growth rates become
214 small. Periodic aeration of the culture was achieved by
215 pumping air through an L-shaped tube sparger assembly.
216 Specifically, an intermittent flow of air at a rate of 0.03 L-air
217 $\text{L}^{-1} \text{min}^{-1}$ was sparged to maintain the oxygen saturation level
218 in the range of 40–70% as monitored using a pO_2 probe
219 (Applikon Biotechnologie B.V., Netherlands). No loss of 4-CP
220 was observed. The feeding bottle was tightly closed and
221 connected to another bottle with the same concentration of 4-
222 CP solution to exclude substance loss by evaporation into the
223 gas phase in the feeding reservoir. The working volume of the
224 bioreactor was maintained at 1600 mL, the pH was held
225 constant at 7.2, and the temperature was 25 $^\circ\text{C}$. A preculture of
226 *A. chlorophenolicus* A6 [10% (v/v)] was used for inoculation.
227 The bioreactors were operated at three dilution rates (D) of
228 0.018, 0.038, and 0.090 h^{-1} corresponding to a hydraulic
229 retention time (HRT) of 3, 1, and 0.46 days, respectively.
230 Dilution rates were only changed after achieving a steady state
231 at a particular D . The steady state was defined by constant cell
232 densities and 4-CP concentrations (<5 and <10% relative
233 variation, respectively) for at least four HRTs. All cultivations
234 were performed in duplicates. Due to the toxicity of 4-CP and
235 intermediates of its catabolic breakdown,⁴³ the cultivation
236 vessels were kept in the safety hood; also, to exclude
237 photodegradation, they were protected from light (cover by
238 aluminum foil).

239 **Measurement of Substrate (4-CP) Concentrations**
240 **and Biomass.** Samples were taken at different time points
241 during batch degradation and continuous operation of the
242 bioreactors. After filtering the samples, concentration measure-
243 ments of 4-CP were conducted using a Prominence HPLC
244 system (Shimadzu Corp., Japan) equipped with a 150 \times 4.6
245 mm Ultracarb 5 μm ODS (30) 60 \AA column (Phenomenex
246 Inc., USA) and UV detector. Details of the HPLC method are

provided in the Supporting Information. To measure the cell
dry weight, samples from chemostats at the steady state were
centrifuged at 4 $^\circ\text{C}$ in a preweighed tube washed with 0.9%
NaCl and dried at 85 $^\circ\text{C}$ to constant weight.³⁰

Determination of Cell Numbers, Viability, and Morphology. Cells were stained with SYBR Green I and propidium iodide to estimate the number of total cells and viable cells by flow cytometry, respectively, as described in Kundu et al.²⁷ The cell concentration measurements were used to define the steady state in the chemostats and for calculating the specific growth rate⁴⁶ in batch cultivation. For morphology, the cells were analyzed on agar glass slides by light microscopy with an AxioScope 2 Plus microscope (Carl Zeiss AG, Germany).⁴⁷

Consumption Rate of 4-CP. The specific substrate consumption rate of 4-CP was represented as q_s , that is, the quotient of substrate consumption rate per hour and biomass present in the vessel ($\text{mg S mg C}_x \text{ h}^{-1}$). q_s was calculated as

$$q_s = \frac{\mu}{Y_{\text{opt}}} \quad (1)$$

where μ is the specific growth rate (in chemostats at steady state, $\mu = D$) and Y_{opt} is the operational yield, that is, mg biomass produced per mg of the substrate consumed where biomass was determined from cell dry weight experimentally as described above. In chemostats, Y_{opt} was determined as described below

$$Y_{\text{opt}} = \frac{X}{S_0 - S} \quad (2)$$

where X is biomass concentration measured at the steady state, S_0 is the 4-CP concentration in the medium, and S is the residual 4-CP concentration at the steady state.

Gas Chromatography Isotope Ratio Mass Spectrometry Analysis of 4-CP Samples in Batch and Chemostats.

Carbon isotope values of the 4-CP (Sigma-Aldrich, Germany) used in the cultivation were determined beforehand using an elemental analyzer coupled with isotope ratio mass spectrometry (EA-IRMS). Details of the method are included in the Supporting Information. For isotope analysis, 10–20 mL of sample volumes was withdrawn from batch and 100–200 mL from chemostats at the steady state. Samples were filtered within 5 min (pore size 0.2 μm , diameter 47 mm; GE Healthcare Ltd., UK) to stop degradation. Degradation during this time was verified to be less than 1% (data not shown). After filtration, 4-CP was extracted with dichloromethane (DCM, 5% of the sample volume, three times, resulting in an overall extraction efficiency of app. 90% and no changes in isotope values). DCM was partly evaporated (not to complete dryness) at room temperature using a gentle nitrogen stream, and finally, 4-CP was reconstituted in 100 μL of DCM. Simultaneously, 1 mL of the medium which was fed to the chemostats was collected, frozen at -80 $^\circ\text{C}$, and dried by lyophilization, and 4-CP was reconstituted in 100 μL of DCM. Controls ensured the absence of isotope fractionation during these operations. Carbon isotope analysis of 4-CP was performed on a gas chromatography-IRMS (GC-IRMS) system (Thermo Fisher Scientific, Waltham, Massachusetts, USA) consisting of a Trace GC with a PAL autosampler (CTC Analytics) equipped with a DB-5 analytical column (30/60 m, 0.25 mm ID, 0.25/1 μm film, Agilent Technologies, Germany) coupled to a Finnigan MAT 253 isotope ratio mass 304

305 spectrometer via a Finnigan GC Combustion III interface
306 (both Thermo Fisher Scientific, Germany).
307 Values of $\delta^{13}\text{C}$ of 4-CP in per mil (‰) are reported relative
308 to PeeDee Belemnite (V-PDB) using the following equation⁴⁹

$$\frac{(R)_x}{(R)_{\text{ref}}} - 1 = \frac{\left(\frac{^{13}\text{C}}{^{12}\text{C}}\right)_x}{\left(\frac{^{13}\text{C}}{^{12}\text{C}}\right)_{\text{ref}}} - 1 = \delta^{13}\text{C} \quad (3)$$

309 where R is the ratio of heavy (^{13}C) and light (^{12}C) carbon
310 isotopes, respectively, in a sample (x) and reference (ref).
311 Determination of $\delta^{13}\text{C}$ values was performed relative to the
312 laboratory CO_2 monitoring gas, which was introduced at the
313 beginning and the end of each analysis run. The laboratory
314 CO_2 was calibrated to the international reference material
315 VPDB by the reference CO_2 standard (RM8563) supplied by
316 the International Atomic Energy Agency. The enrichment
317 factor (ϵ) for batch degradation was calculated using the classic
318 Rayleigh equation^{48,49}

$$\ln \frac{R_t}{R_0} = \frac{\delta^{13}\text{C} + 1}{\delta^{13}\text{C}_0 + 1} = \epsilon \cdot \ln f \quad (4)$$

321 where R_t and R_0 are compound-specific isotope ratios of heavy
322 versus light isotopes at a given time and at the beginning of the
323 reaction, respectively, and f is the fraction of the remaining
324 pollutant in the time course of reaction or degradation. In the
325 case of samples from chemostat experiments where 4-CP was
326 continuously added and the outflow was withdrawn, ϵ was
327 calculated as per the following equation²⁸

$$\epsilon = (\delta^{13}\text{C}_{\text{in}} - \delta^{13}\text{C}_{\text{chemostat}})/(1 - f) \quad (5)$$

329 where δ_{in} and $\delta_{\text{chemostat}}$ refer to carbon isotope ratios of 4-CP in
330 inflow and outflow of the chemostat, respectively, and $f =$
331 ($\text{conc}_{\text{chemostat}}/\text{conc}_{\text{in}}$) denotes the fraction of the residual
332 substrate in the chemostat (eq 2.23 in Hayes, 1983⁵⁰).
333 Samples from each sampling event were split into 3–6
334 technical replicates for isotope measurements. Even though
335 concentrations in the outflow of chemostats were as low as 90
336 $\mu\text{g/L}$, our sampling protocol ensured sufficient mass (1500
337 ppm in the extracts, 1 nmol on-column) for peak amplitudes of
338 2 V ensuring precise isotope analysis (see Figure S9). Overall
339 analytical uncertainty, 2σ of carbon isotope measurements, was
340 $\pm 0.5\%$. For evaluating isotope ratios of samples from batch
341 experiments, measurements were bracketed by those of
342 laboratory standards so that the principle of identical treatment
343 by Werner and Brand⁵¹ could be applied where isotope values
344 are determined against those of precharacterized standards and
345 values are expressed as arithmetic means of 3–6 replicate
346 measurements with their respective standard deviations ($\pm\sigma$).
347 For analysis of samples from chemostat experiments, samples
348 from in- and outflow were measured intermittently so that the
349 enrichment factor for each biological replicate at each dilution
350 rate could be determined as described above (eq 6) from six
351 technical replicates without additional calibration by external
352 standards. These technical replicates did not differ significantly
353 from one another at the 0.05 level for each dilution rate.
354 Hence, the enrichment factors of the two biological replicates
355 were combined and the average is reported.

356 **Lipid Extraction and Membrane Fatty Acid Analysis.**
357 To extract membrane lipids and generate fatty acid methyl
358 esters (FAMES), the “Sherlock Microbial Identification
359 System” was used.⁵² A sample volume of 2 mL was used for

extraction and analysis. In brief, the fatty acids were separated
from the rest of the lipid by saponification followed by
methylation and extraction. The FAMES were analyzed using a
gas chromatograph coupled to a mass spectrometer (GC–MS)
equipped with a split/splitless injector (FinniganTrace Ultra
and Trace DSQ, Thermo Electron Corporation, Waltham, MA,
USA) on a CP-Sil 88 capillary column (Agilent Technologies,
Netherlands; 50 m \times 0.25 mm \times 0.20 μm film). The fatty acids
were identified by their retention time and mass spectrum in
comparison with an authentic standard mix containing
different FAMES (EURISO-TOP GmbH, Saarbrücken,
Germany). The anteiso/iso ratio was calculated as follows

$$\frac{\text{anteiso}}{\text{iso}} \text{ ratio} = \frac{\text{Area}(\text{C15: 0 anteiso})}{\text{Area}(\text{C15: 0 iso})} \quad (6)$$

Details of the method are provided in the Supporting
Information.

Proteomics Analysis. For proteomics analysis, 200 mL of
sample volume was withdrawn from chemostats at steady state
and 20 mL from batch experiments. Details of protein
extraction are reported in our previous publication.²⁷ Ten
micrograms of the whole protein extract from each sample was
used for trypsin digestion using a modified FASP procedure.⁵³
The details of label-free quantification are provided in the
Supporting Information. Normalization of raw abundance data
of all unique peptides allocated to each protein were performed
using Progenesis QI software.

Analysis of normalized abundances of proteins detected
under different cultivation conditions was carried out using the
limma R/Bioconductor package.⁵⁴ A multidimensional scaling
(MDS) plot based on log₂-transformed protein abundances
quantified for different conditions was generated to show the
relationship between different samples. Analysis of differential
protein abundances was performed using the Limma-Voom in
Bioconductor pipeline.^{54,55} The *voom*WithQualityWeights
function was used, which determines both observation-level
and sample-specific weights for subsequent linear modeling.
After *voom* transformation, Empirical Bayes-moderated *t*-
statistics were used to assess the differentially abundant
proteins between different conditions.⁵⁶ The undetected
proteins were handled in the same way as for linear models.⁵⁶
A cutoff in the log fold change (LFC) higher than log₂(2.5)
and a Benjamini–Hochberg⁵⁷-corrected *P*-value of <0.05 were
applied for the proteins to be differentially abundant during the
pairwise comparison between different conditions. Normalized
protein abundance of each protein was converted to *z*-score
using the transformation $[x - \text{mean}]/\text{SD}$, where x is one
protein in the data set population and SD is the standard
deviation. Hierarchical clustering of the *z*-scores for the
differentially abundant proteins and all quantified proteins
was performed using “Euclidean distance” as a distance
function and was visualized as heat maps with the *seaborn*
package.⁵⁸

RESULTS AND DISCUSSION

**Chemostat Cultivation Revealed That Degradation
Activity Was Downregulated at Low Concentrations.** 4-
CP was degraded in batch ($S_0 = 220 \text{ mg L}^{-1}$) up to 82% within
55 h (Supporting Information, Figure S2). This confirms that
Arthrobacter chlorophenolicus A6 can withstand high and toxic
concentrations of 4-CP as suggested by Westerberg et al.⁵ In
addition, 4-CP is known to be inhibitory to *A. chlorophenolicus*

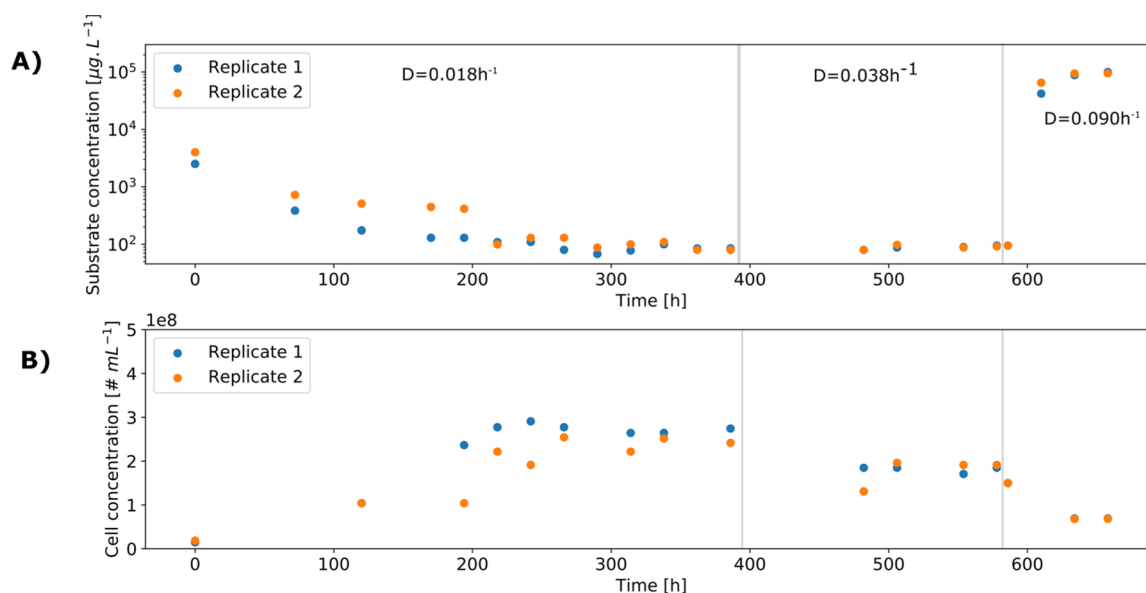


Figure 1. Chemostat cultivation reveals that degradation activity was regulated on the enzyme level. (A) Concentration of residual 4-CP at different dilution rates in chemostats. (B) Cell numbers per milliliter at different dilution rates.

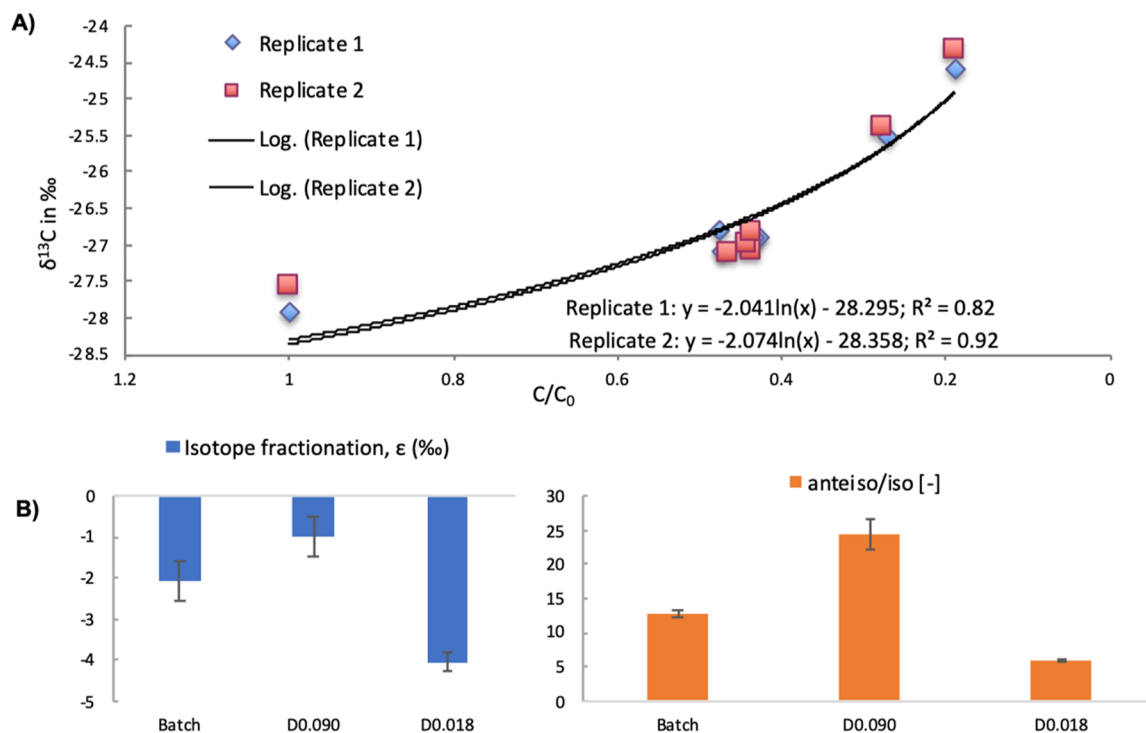


Figure 2. Higher isotope fractionation in chemostat cultivation indicates that 4-CP degradation at low concentrations was not mass transfer-limited. (A) Isotope fractionation (ϵ) in batch (high concentration data point) was determined according to the Rayleigh equation (eq 5). (B) Isotope fractionation at different dilution points in chemostats. Isotope fractionation in a chemostat was determined by the difference of the isotope values ($\delta^{13}\text{C}$) of inflow and outflow (eq 6). Error bars indicate the standard deviation of isotope analysis of samples. A ratio of anteiso vs iso fatty acid shows higher membrane permeability at high concentrations.

419 A6,³⁷ where substrate inhibition follows a fundamental
 420 biological regulatory mechanism.⁵⁹ The regulating effect has
 421 also been reported in the microbial growth rate which—in
 422 contrast to classical Monod growth kinetics—was found to
 423 become lower at high concentrations^{60,61} and even the lag
 424 phase of the microbial growth curve was found to be extended
 425 at high inhibitory concentrations.^{5,60} Analogous observations

were made in this study and could be modeled by Haldane 426
 kinetics (see Figures S2 and S3). 427

After observing an expected regulating effect at high 4-CP 428
 concentrations (mg L^{-1} range) in batch experiments, we 429
 explored adaptation in the low-concentration regime in 430
 chemostat experiments (Figure 1A,B). The residual steady- 431 f1
 state 4-CP concentration in chemostats operated at a D of 432
 0.018 h^{-1} was $90 \pm 10 \mu\text{g L}^{-1}$ or $0.7 \pm 0.1 \mu\text{M}$, which is much 433

434 smaller than the Monod constant of $K_s = 0.012$ mM estimated
435 from kinetic modeling (Supporting Information, Figure S3).
436 The viable cell count at this concentration was $\sim 2.22 \pm 0.32 \times$
437 10^8 cells mL^{-1} . Remarkably, changing the D to 0.038 h^{-1} did
438 not introduce significant changes in the 4-CP concentration
439 (95 ± 10 $\mu\text{g L}^{-1}$) at the steady state (Figure 1A) neither was
440 an apparent change in the biomass in terms of cell
441 concentration ($1.92 \pm 0.32 \times 10^8$ cells mL^{-1}) observed
442 (Figure 1B). This is in stark contrast to the classical behavior
443 of chemostat experiments where residual substrate concen-
444 trations decrease with a decrease in D .¹⁷ Previously, this kind
445 of behavior was observed in benzoate degradation where no
446 significant change in residual concentration was observed after
447 changing D , an observation which was attributed to regulation
448 of enzymatic turnover by altered degradation protein
449 abundance.¹⁸ Hence, the fact that the same residual
450 concentration was observed even after doubling D implies
451 that degradation activity at low concentrations of 4-CP must
452 have been regulated leading to slower turnover and higher
453 residual concentrations than expected—also in comparison
454 with the batch degradation experiment, 4-CP was completely
455 degraded (Supporting Information, Figure S2).

456 It was only at an extremely high dilution rate of $D = 0.09$ h^{-1}
457 that steady-state cell concentrations decreased to 6.83 ± 0.12
458 $\times 10^7$ cells mL^{-1} and a stark increase in 4-CP concentrations to
459 88 ± 8 mg L^{-1} (0.68 mM) was finally observed (Figure 1A,B).
460 Since under these conditions, residual 4-CP concentrations (S)
461 greatly exceeded the Haldane inhibition constant $K_i = 12.0$ mg
462 L^{-1} from kinetic modeling (Supporting Information, Figure
463 S3), this inhibitory effect is fully consistent with our
464 observation of inhibition at high substrate concentrations
465 from batch. Combined evidence from batch and chemostats
466 therefore suggests that 4-CP degradation was not only
467 inhibited at high 4-CP concentrations—as known from the
468 literature⁵⁹ and modeled by Haldane kinetics (Supporting
469 Information, Figure S3)—but we discovered that turnover was
470 in addition decreased by regulation of enzyme activity at low
471 concentrations. In a next step, we therefore explored whether
472 such a regulation of enzyme activity was associated with
473 changes in isotope fractionation.

474 **Pronounced Isotope Fractionation in Chemostats**
475 **Indicates That 4-CP Degradation Was Not Strongly**
476 **Mass Transfer-Limited at Low (90 $\mu\text{g L}^{-1}$) Concen-**
477 **trations.** In a batch experiment starting at high concentrations
478 ($c_0 = 220$ mg L^{-1}), isotope analysis of 4-CP at different
479 degradation time points showed significant changes in isotope
480 values $^{13}\text{C}/^{12}\text{C}$ ($\delta^{13}\text{C}$) in the remaining 4-CP (Figure 2A).
481 Determination of the carbon isotope enrichment factor
482 according to the Rayleigh equation resulted in a value of $\epsilon =$
483 $-2.1 \pm 0.5\%$. No isotope fractionation was observed in sterile
484 controls which confirmed that no isotope fractionation was
485 introduced by steps of extraction and reconstitution of
486 samples. An even smaller extent of isotope fractionation of ϵ
487 $= -1.0 \pm 0.5\%$ was obtained in chemostats at very high
488 dilution $D = 0.090$ h^{-1} and a high residual substrate
489 concentration of 88 mg L^{-1} . In contrast, in chemostats at D
490 0.018 h^{-1} with a much lower residual concentration of 90 ± 10
491 $\mu\text{g L}^{-1}$, the isotope enrichment factor of 4-CP in chemostats
492 was significantly higher ($\epsilon = -4.1 \pm 0.2\%$, Figure 2B). This
493 value even stands out when comparing it to carbon isotopic
494 enrichment factors reported for biodegradation of other
495 phenolic substrates transformed through aromatic ring
496 oxidation such as of phenol ($\epsilon = -1.5 \pm 0.1\%$),⁴⁴ cresol (ϵ

$= -1.4 \pm 0.2\%$),⁴⁴ 2-nitrophenol ($\epsilon = -1.2 \pm 0.1\%$),⁶² 5-
497 methyl-2-nitrophenol ($\epsilon = -1.3 \pm 0.2\%$),⁶² or trichlorinated
498 phenols ($\epsilon = -0.5$ to $+0.3\%$).⁶³ The initial step in degradation
499 of 4-CP in *A. chlorophenolicus* A6 is catalyzed by two
500 monooxygenases.⁴³ Hence, this value may be compared to
501 carbon isotope fractionation in ring monooxygenation from
502 enzyme assays where a possible influence of the cell membrane
503 was eliminated, such as of 2-nitrophenol ($\epsilon = -1.4 \pm 0.1\%$),⁶²
504 5-methyl-2-nitrophenol ($\epsilon = -1.5 \pm 0.2\%$),⁶² 4-hydroxyph-
505 nylacetate ($\epsilon = -1.1 \pm 0.1\%$),⁶⁴ and 4-hydroxybenzoate ($\epsilon =$
506 $-0.1 \pm 0.1\%$).⁶⁴ Again, these reported values are smaller than
507 the isotope fractionation observed in our study. It is well-
508 recognized and has been demonstrated in an illustrative study
509 by Wijker et al. that intrinsic isotope effects may already be
510 masked on the enzyme level—depending on the presence of
511 “bold” versus “cautious” monooxygenases—so that these
512 values of enzymes and microorganisms likely do not reflect
513 the intrinsic isotope effect of the underlying biochemical
514 reaction.⁶⁴ To compare it with tabulated kinetic isotope effects
515 of unmasked reactions, we therefore considered that our
516 observed enrichment factor $\epsilon = -4.1 \pm 0.2\%$ represents a
517 compound average and that 4-CP contains six carbon atoms so
518 that a position-specific apparent kinetic isotope effect can
519 tentatively be estimated as $\text{AKIE} = 1/(-0.0041 \cdot 6 + 1) =$
520 1.025 .⁶⁵ This value falls toward the upper end of the range of
521 unmasked kinetic isotope effects reported for abiotic C=C
522 bond oxidation (1.011 to 1.024 , Table 2 Elsner et al.⁶⁵). We
523 can, therefore, conclude (i) that the degradation of 4-CP at low
524 concentrations was not significantly mass transfer-limited and
525 (ii) that it even represented the intrinsic isotope effect of the
526 underlying biochemical reaction inside the enzyme—other-
527 wise, this intrinsic isotope effect would have been masked. 528

529 This increase in isotope fractionation at lower concen-
530 trations, however, is in stark contrast with results from our
531 recent study on atrazine degradation, where a dramatic
532 decrease in isotope fractionation was observed when substrate
533 concentrations fell below 60 $\mu\text{g L}^{-1}$.²⁸ A direct comparison is
534 difficult because—in contrast to atrazine degradation by *A.*
535 *aureus* TC1—the regulation of enzyme activity in *A.*
536 *chlorophenolicus* A6 prevented us from reaching 4-CP
537 concentrations below 85 $\mu\text{g L}^{-1}$ in our chemostat experiments:
538 when lowering the dilution rate, cell-specific activity also
539 declined so that concentrations remained at the same level,
540 even though a longer residence time was available for
541 degradation. Nonetheless, we observed (i) that the intrinsic
542 isotope effect of the enzyme reaction was strongly expressed at
543 low (90 ± 10 $\mu\text{g L}^{-1}$) concentrations; (ii) that enzyme activity
544 appeared to be strongly regulated under these circumstances;
545 and (iii) that much smaller isotope fractionation was observed
546 at higher concentrations in batch and chemostats. This
547 observation is in contrast to theoretical predictions that
548 smaller isotope fractionation is expected at lower rather than at
549 higher concentrations.^{15,16} It therefore highlights a novel type
550 of regulation at low concentrations suggesting either a switch
551 in metabolic pathways and/or that an interplay between
552 changes in membrane permeability and enzyme activity may be
553 at work as hypothesized in the Introduction. In a next step, we
554 therefore considered evidence from the analysis of membrane
555 fatty acids and proteomics to explore a possible role of
556 membrane composition and the regulation of enzyme
557 expression.

558 **Fatty Acid Analysis Gives Evidence of Smaller**
559 **Membrane Permeability at Low Concentrations.** The

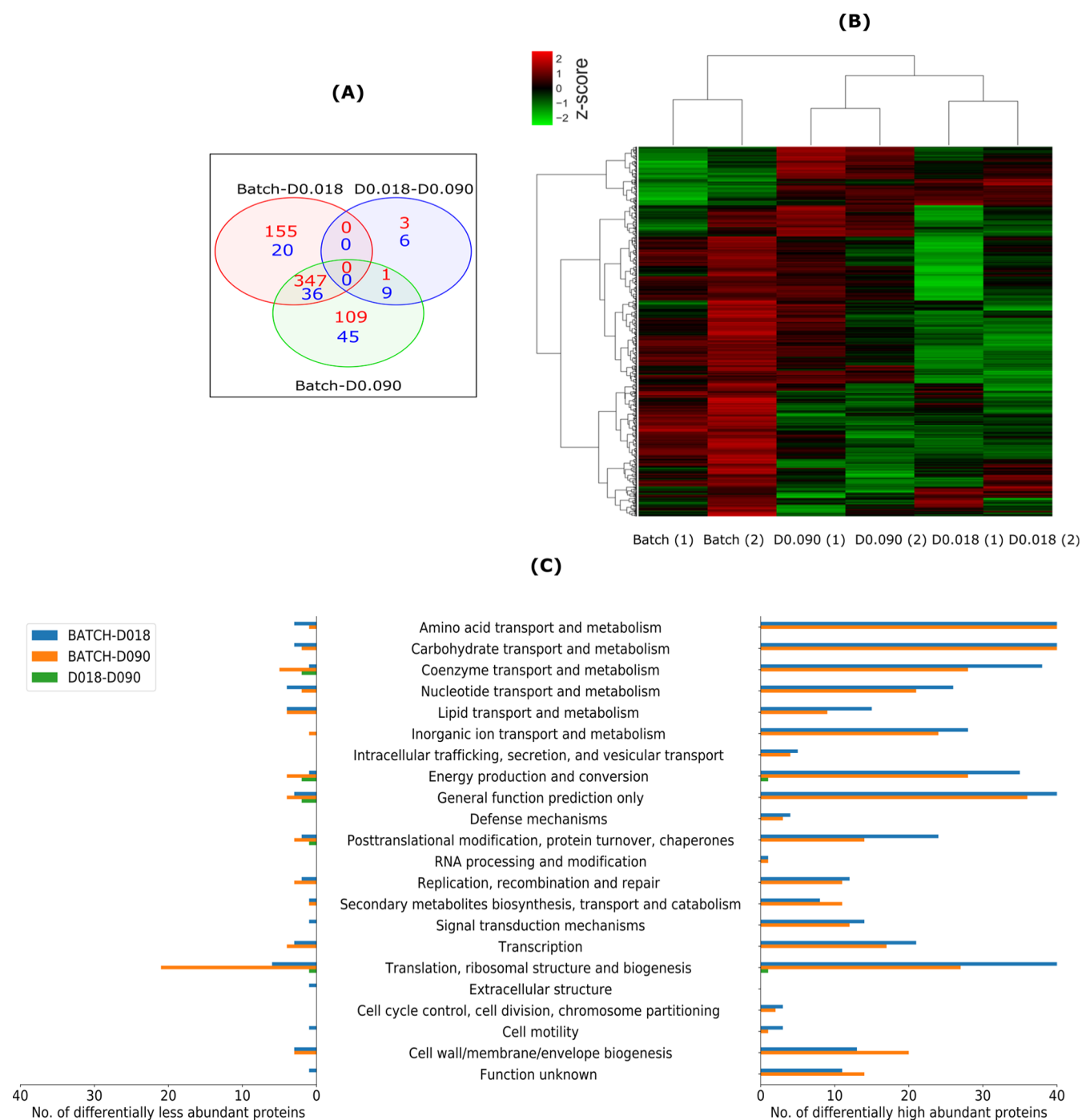


Figure 3. Physiological adaptation at different concentrations in chemostats and batch. (A) Venn diagram illustrates differentially abundant proteins between the three comparison pairs—batch vs chemostat at D0.018 (Batch–D0.018), D0.018 vs chemostat at a dilution rate of 0.090 h⁻¹ (D0.018–D0.090), and batch vs D0.090 (Batch–D0.090). Numbers in red represent significantly highly abundant proteins and those in blue represent proteins of significantly low abundance. (B) Heat map representing the clustering of 731 significantly abundant proteins at batch, D0.018, and D0.09. Protein abundance is displayed in the heat map as z-scores (i.e., calculated based on how many SD units a protein’s abundance is away from the mean abundance derived from all conditions) in the range between 2 (of significantly higher abundance, red) and –2 (of significantly lower abundance, green). Each batch and chemostat cultivation was performed in replicates as indicated by dilution rates in the brackets below the heat map. (C) Distribution of overlapping significantly high- and low-abundant proteins across COG categories in batch, D0.018, and D0.09. First seven COG categories contained proteins for transport and were highly abundant (present at the right side of the tornado plot) in batch compared to D0.018 indicating that the transport of molecules was slow at D0.018.

transport across the membrane of bacterial cells is affected by its physical properties, especially by its fatty acid content.⁶⁶ The fatty acid content of a cell membrane can change as a result of physiological adaptation.^{36,37,40,67} In *A. chlorophenolicus* A6, the predominating fatty acids are iso-pentadecanoic

(iso-C15:0) and anteiso-pentadecanoic (anteiso-C15:0).⁵ It is well-established that the ratio of anteiso/iso controls the fluidity or permeability of the membrane, where a high anteiso content makes the membrane more fluid.³⁷ Surprisingly, measurement of membrane fatty acids showed a greater

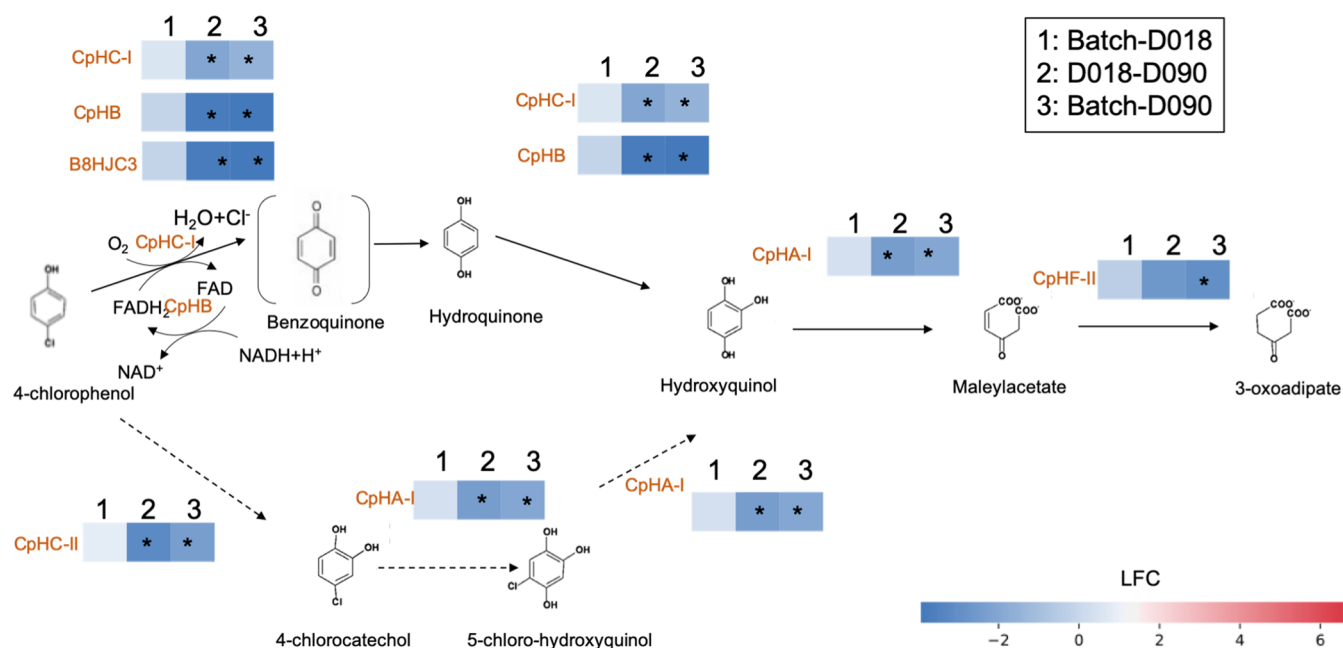


Figure 4. 4-CP degradation pathway adapted from the literature.^{43,71,72,77} Three pairwise comparison groups were created as indicated by the numbers 1, 2, and 3. 1: Batch vs chemostat at a dilution rate of 0.018 h^{-1} (batch-D018). 2: Chemostat at a dilution rate of 0.018 h^{-1} vs chemostat at a dilution rate of 0.090 h^{-1} (D018-D090). 3: Batch vs chemostat at a dilution rate of 0.090 h^{-1} (batch-D090). Different colors represent the LFC in specific proteins from a pairwise comparison between chemostats and batch. Symbols (*) indicate proteins of differential abundance, where the criteria for significant differences were a P -value of <0.05 together with a cutoff LFC of $\log_2(2.5)$. The dotted line indicates the postulated pathway, and the brackets indicate the hypothetical intermediate.

570 anteiso-to-iso ratio in batch indicating that the cell membrane
571 was more permeable than at low concentrations in chemostats
572 (Figure 2B). This is contrary to the observation of Unell et
573 al.,³⁷ where a lower anteiso-to-iso ratio was observed at high 4-
574 CP concentrations—however, under growth on yeast extract
575 with spiked 4-CP so that the results are not directly
576 comparable to our findings. It also contrasts recent findings
577 by Wunderlich et al.⁴⁵ who observed that higher 4-CP
578 concentrations resulted in more rigid membranes in *Thaurera*
579 *aromatica* (higher degree of fatty acid saturation), entailing
580 smaller $^{15}\text{N}/^{14}\text{N}$ isotope fractionation during nitrate reduction.
581 It is noteworthy that our results represent a specific case where
582 the phenolic compound was used as a growth substrate. We
583 speculate that cells may have abstained from making the
584 membrane rigid so that permeation would not be slowed when
585 an efficient enzyme machinery was in place for catabolic
586 breakdown. Since 4-CP is more lipophilic than nonsubstituted
587 phenols,³⁷ permeation is likely mediated by diffusion. Never-
588 theless, to understand the possible role of transporters in the
589 degradation, we looked into the expression of proteins related
590 to transport.

591 Proteomics Reveals Significantly Lower Abundance 592 of Transport-Related Proteins at Low Concentrations.

593 Microorganisms are known to physiologically adapt to different
594 substrate conditions, for example, by upregulating specific
595 enzymes or transporters, which is generally reflected in the
596 proteome state of the cells.^{27–29,68} The proteome state of the
597 cells was analyzed in chemostats at D 0.018 and D 0.09 and in
598 batch. In total, 1404 proteins were quantified which
599 corresponds to $\sim 31\%$ coverage of total predicted protein-
600 coding genes in *A. chlorophenolicus* A6 and 1201 proteins were
601 quantified in all the samples (Supporting Information, Table
602 S1). During pairwise comparisons of three cultivation
603 conditions, 731 differentially abundant proteins (either up/

604 downregulated) (Figure 3A) were observed. Hierarchical
605 clustering of differentially abundant proteins shows that
606 many proteins in batch and at D0.09 had a significantly higher
607 abundance (z -score around 2) which were less abundant at
608 D0.018 suggesting an adaptation at the cellular level in
609 response to low concentrations (Figure 3B). To perform a
610 functional interpretation, these differentially abundant proteins
611 were linked to clusters of orthologous group categories
612 (COGs)⁶⁹ (Figure 3C, Supporting Information, Tables S2–
613 S4). Specific transporters for 4-CP are not known. However,
614 putative transporters which might play a role in 4-CP
615 permeation were highly abundant at high concentrations
616 such as the putative ligand-binding sensor protein (B8H8Y4)
617 (Supporting Information, Tables S2 and S4). This suggests
618 that in the case of transporter-mediated permeation, mass
619 transfer might have been accelerated at high concentrations at
620 batch compared to low concentrations. In this study, therefore,
621 both the fatty acid analysis and proteomics data indicate that
622 the lower isotope fractionation at high concentrations in
623 chemostats is not caused by a less-permeable cell membrane
624 but must have other reasons. In a next step, proteomics was
625 therefore evaluated to explore regulation on the level of
626 enzyme expression.

**Differential Expression of Proteins Related to 4-CP
627 Degrading Enzymes at Low Concentrations.** As discussed
628 above, the high isotope fractionation ($\epsilon = -4.1 \pm 0.2\text{‰}$) in
629 chemostats (D0.018) gives unequivocal evidence that
630 enzymatic turnover was slow relative to mass transfer at low
631 concentrations—otherwise, intrinsic isotope effects would not
632 have been so strongly expressed. When interpreting this value
633 in comparison with the lower observable isotope fractionation
634 at high concentrations in batch and chemostats at D0.09, the
635 decisive step is the enzyme reaction of the initial irreversible
636 transformation. Compared to atrazine transformation by *A.* 637

638 *aureus* TC1, 4-CP transformation by *A. chlorophenicus* A6
639 is more complex because it may involve two possible initial
640 pathways,⁴³ which are encoded by a chlorophenol degradation
641 (cph) gene cluster involving different proteins (Figure 4,
642 Supporting Information, Table S5). One initial oxidative
643 degradation pathway of 4-CP is catalyzed by CphCI and
644 CphB which—together with flavin reductase (B8HJC3)—
645 form a two-component flavin-diffusible monooxygenase (TC-
646 FDM).^{43,70–72} CphB reduces FAD to FADH₂ via NADH,
647 whereas CphCI uses FADH₂ to activate molecular O₂ for
648 oxidation of 4-CP to hydroxyquinone.^{71,72} The second
649 degradation pathway is catalyzed by the CphCII protein
650 which has been postulated to oxidize 4-CP to 4-chloroca-
651 techol.⁴³ Here, the degradation mechanism has not been
652 elucidated yet. Consequently, the turnover of 4-CP can be the
653 result of two parallel transformations catalyzed by CphCI and
654 CphCII, and the observable isotope fractionation may be the
655 weighted average of both, where it would mostly reflect the
656 predominant pathway. The observation that breakdown by
657 different enzymes causes different isotope effects in organic
658 pollutants has been made previously for dioxygenases in
659 nitroaromatic compound oxidation⁷³ or for ring versus methyl
660 group oxidation of toluene.⁷⁴

661 Hence, when interpreting the smaller value of ϵ at high
662 concentrations in batch in comparison with the large ϵ in
663 chemostats at D0.018, the modulated ϵ may either be evidence
664 of masked isotope fractionation due to mass transfer or the
665 result of a metabolic shift between the two initial pathways of
666 Figure 4 leading to a different weighted average of isotope
667 effects from two different enzymes. In this case, one would
668 expect regulation of one enzymatic pathway relative to the
669 other at high versus low concentrations (CphCI vs CphCII).
670 Direct observation of either pathway was not possible
671 because our chemical analysis was not optimized to measure
672 the respective short-lived intermediates (hydroxyquinone vs 4-
673 chlorocatechol). However, to understand the regulation on the
674 degradation of 4-CP at low concentrations, proteins related to
675 the 4-CP degradation pathway could be compared between
676 D0.018, D0.09, and batch (Figure 4). We observed that CphCI
677 and CphCII were both differentially less abundant at D0.018
678 compared to D0.090 (Supporting Information, Table S5,
679 Figure 4). This indicates that downregulation of enzymes is a
680 possible reason for the higher isotope fractionation observed at
681 low concentrations. Alternatively, a shift in degradation
682 pathways might play a role. Indeed, abundance of CphCI
683 was fourfold reduced, whereas CphCII was eightfold less
684 abundant (Supporting Information, Table S5). Both CphCI
685 and CphCII are inducible not constitutive,⁴² and evidence
686 from previous work suggests that both pathways were co-
687 occurring at high concentrations (no kinetic preference).⁴³
688 Hence, the expression level of CphCI and CphCII might also
689 contribute to a dominance of one degradation pathway. In this
690 study, the relative abundance of CphCI was higher than
691 CphCII under all conditions. However, a small shift in the ratio
692 of CphCI/CphCII—about half from D018 (202:1) and batch
693 (159:1) to D090 (90:1)—was observed (Supporting Informa-
694 tion, Table S5), which might also produce a small shift in
695 degradation pathways. Hence, our analysis highlights physio-
696 logical adaptation on the enzyme expression level—both with
697 respect to total abundance of catabolic enzymes (CphCI and
698 CphCII) and with respect to a possible shift in metabolic
699 pathways (CphCI and CphCII) at low concentrations.

This total abundance (CphCI and CphCII) also explains the
observed regulation on 4-CP turnover in chemostats, which
decreased with lower dilution rates leading to the same residual
substrate concentration at different dilution rates, Figure 1, and
the situation that two different q_s were observed at the same
residual concentrations (0.66 ± 0.12 vs 1.54 ± 0.65 mg S mg
 $C_x^{-1} h^{-1}$ at D of 0.018 and 0.038 h^{-1} , respectively, See
Supporting Information, Table S6). At high D (0.09), a high q_s
(6.14 ± 0.88 mg S⁻¹ mg C_x h⁻¹) was observed indicating that
degradation became faster at high concentrations and became
smaller at low concentrations in chemostats, consistent with
our conclusions about enzyme activity regulation at low
concentrations mentioned above. Specifically, when the
feeding pump was stopped, only very slow degradation was
observed over 60 min in chemostats at a residual (=effluent)
concentration of 90 ± 5 $\mu\text{g L}^{-1}$ (Supporting Information,
Figure S5). This is in contrast to atrazine degradation, where
we observed rapid degradation of atrazine in chemostats at a
residual (=effluent) concentration of 60 $\mu\text{g L}^{-1}$.²⁸ Besides the
downregulation of proteins (Figure 3), the overall reduced
metabolism was also reflected in the morphology of cells
(Supporting Information, Figure S4).

Environmental Significance. In natural oligotrophic
environments such as groundwater, heterotrophic bacteria
feed on a multitude of naturally occurring organic compounds
that have in common that they occur only in small
concentrations. Hence, understanding bacterial regulation
and adaptation under such low-energy conditions is of general
importance—as much for the persistence of organic matter in
carbon budgeting, as for bioremediation of low-level chemical
pollution. To explore possible underlying patterns of
adaptation, this study has focused on degradation of one
substrate (4-CP) by one strain in a setup of deliberately
reduced complexity. Even though this experimental design
does not directly mimic natural groundwater conditions, it has
the advantage that it enables a relevant generic process
understanding by allowing us to combine evidence from CSIA,
membrane fatty acid analysis, and the analysis of the proteome
state of the cells. This multidisciplinary approach revealed (i)
that the enzymatic turnover inside bacteria of the studied strain
A. chlorophenicus A6 was regulated at multiple levels at low
concentrations ($\mu\text{g L}^{-1}$) including membrane composition, as
well as differential expression of enzymes and/or a possible
shift in metabolic pathways, and (ii) that this regulation
resulted in a situation that substrate supply through the cell
membrane did not become rate-limiting at low concentrations
but that rather enzyme activity inside the cell was down-
regulated first. Since this observation is in stark contrast to the
observation of mass transfer limitation in low-level atrazine
degradation by *A. aureus* TC1²⁸ or of 2,6-dichlorobenza-
mid degradation by *Aminobacter* sp. MSH1,⁷⁵ the present
study reveals a different pattern of microbial adaptation to low
concentrations: bacteria downregulated their enzymatic
activity instead of running into limited substrate supply.
Hence, the pattern observed here reveals another “end-
member behavior” on the scale of physiological adaptation of
degrading bacteria that can be expected in low-energy
environments. Remarkably, this physiological limitation was
observed at a concentration around 90 $\mu\text{g L}^{-1}$. Considering
that $\Delta_R G^{\circ} \text{cat} = -111 \pm 5$ kJ·mol⁻¹ and that the observed
specific substrate consumption rate observed was 0.66 mg S g
 $C_x^{-1} \cdot h^{-1}$, this concentration is much higher than the minimum
substrate concentration required for maintenance of cells’

763 viability.⁷⁶ Cells can physiologically adapt under extremely low
764 energy fluxes which will enable moving to much lower
765 concentrations with a near-zero growth rate.²⁷ Nonetheless,
766 in this study, degradation was observed to become slow already
767 at 90 $\mu\text{g L}^{-1}$ indicating that microbial adaptation by enzyme
768 regulation would curb bioremediation efforts—or utilization of
769 organic matter—at low concentrations. Based on this insight,
770 we conclude that bioaugmentation approaches would seem
771 most promising when they rely on bacteria that maintain their
772 intrinsic enzyme activity high so that they run into mass
773 transfer limitations as an ultimate physical limit before
774 downregulating their metabolism. The discovery of such
775 specific physiological adaptation in degrading bacteria
776 emphasizes the need for a knowledge base for management
777 of bioremediation of different pollutants that account for
778 bacterial adaptation. In future studies, it will, hence, be
779 important to study degradation of other contaminants by
780 different microorganisms to better understand limitations of
781 mass transfer versus enzymatic turnover on micropollutant
782 degradation—or organic substrates in general—at low
783 concentrations and design strategies to overcome them.

784 ■ ASSOCIATED CONTENT

785 ■ Supporting Information

786 The Supporting Information is available free of charge at
787 <https://pubs.acs.org/doi/10.1021/acs.est.1c04939>.

788 Materials and methods; HPLC method for 4-CP
789 concentration measurement; estimation of growth
790 kinetic parameters; EA-IRMS measurement for deter-
791 mination of reference values; method for analysis of the
792 carbon isotope in 4-CP samples; lipid extraction and
793 membrane fatty acid analysis; proteomics analysis;
794 schematic diagram of the custom-made bioreactor used
795 in this study; degradation of 4-CP and cell concentration
796 in a batch cultivation experiment; observed specific
797 growth rate at different residual 4-CP concentrations in
798 batch; degradation profile of 4-CP at 95 $\mu\text{g L}^{-1}$ shows
799 slow enzymatic turnover; change in morphology at
800 different dilution points in chemostats and batch;
801 NMDS of all conditions used for proteomics analysis;
802 heat map representing the clustering of quantified
803 proteins; Voom transformation of the proteomics data;
804 GC-IRMS chromatogram of low-concentration extracts;
805 proteomics data analysis; and biomass and yield
806 measured at different dilution rates after achieving
807 steady states in chemostats (PDF)

808 ■ AUTHOR INFORMATION

809 Corresponding Authors

810 **Kankana Kundu** – *Institute of Groundwater Ecology,*
811 *Helmholtz Zentrum Munchen, 85764 Neuherberg, Bavaria,*
812 *Germany; Center for Microbial Ecology and Technology*
813 *(CMET), Faculty of Bioscience Engineering, University of*
814 *Ghent, 9000 Ghent, Belgium; [orcid.org/0000-0001-](https://orcid.org/0000-0001-7147-157X)*
815 *[7147-157X](https://orcid.org/0000-0001-7147-157X); Email: kankanakundu@gmail.com*

816 **Martin Elsner** – *Institute of Groundwater Ecology, Helmholtz*
817 *Zentrum Munchen, 85764 Neuherberg, Bavaria, Germany;*
818 *Chair of Analytical Chemistry and Water Chemistry,*
819 *Technical University of Munich, D-85748 Garching,*
820 *Germany; orcid.org/0000-0003-4746-9052; Phone: +49*
821 *89 2180-78232; Email: m.elsner@tum.de*

822 Authors

Aileen Melsbach – *Institute of Groundwater Ecology,*
823 *Helmholtz Zentrum Munchen, 85764 Neuherberg, Bavaria,*
824 *Germany; Chair of Analytical Chemistry and Water*
825 *Chemistry, Technical University of Munich, D-85748*
826 *Garching, Germany*

Benjamin Heckel – *Institute of Groundwater Ecology,*
827 *Helmholtz Zentrum Munchen, 85764 Neuherberg, Bavaria,*
828 *Germany*

Sarah Schneidemann – *Center for Microbial Ecology and*
829 *Technology (CMET), Faculty of Bioscience Engineering,*
830 *University of Ghent, 9000 Ghent, Belgium*

Dheeraj Kanapathi – *Institute of Groundwater Ecology,*
831 *Helmholtz Zentrum Munchen, 85764 Neuherberg, Bavaria,*
832 *Germany*

Sviatlana Marozava – *Institute of Groundwater Ecology,*
833 *Helmholtz Zentrum Munchen, 85764 Neuherberg, Bavaria,*
834 *Germany*

Juliane Merl-Pham – *Core Facility Proteomics, Helmholtz*
835 *Zentrum München, 80939 Munich, Germany*

836 Complete contact information is available at:
837 <https://pubs.acs.org/10.1021/acs.est.1c04939>

838 Author Contributions

839 The manuscript was written through contributions of all
840 authors. All authors have given approval to the final version of
841 the manuscript.

842 Notes

843 The authors declare no competing financial interest.

844 ■ ACKNOWLEDGMENTS

845 This work was funded by an ERC consolidator grant
846 (“MicroDegrad”, grant no. 616861) awarded by the European
847 Research Council.

848 ■ REFERENCES

- 849 (1) Fenner, K.; Canonica, S.; Wackett, L. P.; Elsner, M. Evaluating
850 Pesticide Degradation in the Environment: Blind Spots and Emerging
851 Opportunities. *Science* **2013**, *341*, 752–758.
- 852 (2) Shannon, M. A.; Bohn, P. W.; Elimelech, M.; Georgiadis, J. G.;
853 Mariñas, B. J.; Mayes, A. M. Science and Technology for Water
854 Purification in the Coming Decades. *Nature* **2008**, *452*, 301–310.
- 855 (3) Shao, Y.; Chen, Z.; Hollert, H.; Zhou, S.; Deutschmann, B.;
856 Seiler, T.-B. Toxicity of 10 Organic Micropollutants and Their
857 Mixture: Implications for Aquatic Risk Assessment. *Sci. Total Environ.*
858 **2019**, *666*, 1273–1282.
- 859 (4) Strong, L. C.; Rosendahl, C.; Johnson, G.; Sadowsky, M. J.;
860 Wackett, L. P. *Arthrobacter aurescens* TC1 Metabolizes Diverse s
861 -Triazine Ring Compounds. *2002*, *68* (12), 5973–5980
862 DOI: [10.1128/aem.68.12.5973-5980.2002](https://doi.org/10.1128/aem.68.12.5973-5980.2002)
- 863 (5) Westerberg, K.; Elväng, A. M.; Stackebrandt, E.; Jansson, J. K.
864 *Arthrobacter Chlorophenolicus* Sp. Nov., a New Species Capable of
865 Degrading High Concentrations of 4-Chlorophenol. *Int. J. Syst. Evol.*
866 *Microbiol.* **2000**, *50*, 2083–2092.
- 867 (6) Kolvenbach, B. A.; Helbling, D. E.; Kohler, H.-P. E.; Corvini, P.
868 F.-X. Emerging Chemicals and the Evolution of Biodegradation
869 Capacities and Pathways in Bacteria. *Curr. Opin. Biotechnol.* **2014**, *27*,
870 8–14.
- 871 (7) Arrieta, J. M.; Mayol, E.; Hansman, R. L.; Herndl, G. J.; Dittmar,
872 T.; Duarte, C. M. Dilution Limits Dissolved Organic Carbon
873 Utilization in the Deep Ocean. *Science* **2015**, *348*, 331–333.
- 874 (8) Hofmann, R.; Griebl, C. DOM and Bacterial Growth
875 Efficiency in Oligotrophic Groundwater: Absence of Priming and
876 Co-Limitation by Organic Carbon and Phosphorus. *Aquat. Microb.*
877 *Ecol.* **2018**, *81*, 55–71.

- 884 (9) Egli, T. How to Live at Very Low Substrate Concentration. 885 *Water Res.* **2010**, *44*, 4826–4837.
- 886 (10) Griebler, C.; Mindl, B.; Slezak, D. Combining DAPI and SYBR 887 Green II for the Enumeration of Total Bacterial Numbers in Aquatic 888 Sediments. *Int. Rev. Hydrobiol.* **2001**, *86*, 453–465.
- 889 (11) Whitman, W. B.; Coleman, D. C.; Wiebe, W. J. Prokaryotes: 890 The Unseen Majority. *Proc. Natl. Acad. Sci. U.S.A.* **1998**, *95*, 6578– 891 6583.
- 892 (12) Tabor, P. S.; Neihof, R. A. Improved Microautoradiographic 893 Method to Determine Individual Microorganisms Active in Substrate 894 Uptake in Natural Waters. *Appl. Environ. Microbiol.* **1982**, *44*, 945– 895 953.
- 896 (13) Teira, E.; Reinthaler, T.; Pernthaler, A.; Pernthaler, J.; Herndl, 897 G. J. Combining Catalyzed Reporter Deposition-Fluorescence in Situ 898 Hybridization and Microautoradiography to Detect Substrate 899 Utilization by Bacteria and Archaea in the Deep Ocean. *Appl.* 900 *Environ. Microbiol.* **2004**, *70*, 4411–4414.
- 901 (14) Bosma, T. N. P.; Middeldorp, P. J. M.; Schraa, G.; Zehnder, A. 902 J. B. Mass Transfer Limitation of Biotransformation: Quantifying 903 Bioavailability. *Environ. Sci. Technol.* **1996**, *31*, 248–252.
- 904 (15) Thullner, M.; Kampara, M.; Richnow, H. H.; Harms, H.; Wick, 905 L. Y. Impact of Bioavailability Restrictions on Microbially Induced 906 Stable Isotope Fractionation. 1. Theoretical Calculation. *Environ. Sci.* 907 *Technol.* **2008**, *42*, 6544–6551.
- 908 (16) Kampara, M.; Thullner, M.; Richnow, H. H.; Harms, H.; Wick, 909 L. Y. Impact of Bioavailability Restrictions on Microbially Induced 910 Stable Isotope Fractionation. 2. Experimental Evidence. *Environ. Sci.* 911 *Technol.* **2008**, *42*, 6552–6558.
- 912 (17) Heijnen, J. J. Bioenergetics of Microbial Growth. *Encyclopedia* 913 *of Industrial Biotechnology: Bioprocess, Bioseparation, and Cell* 914 *Technology*; Wiley Online Library, 1999.
- 915 (18) Trautwein, K.; Lahme, S.; Wöhlbrand, L.; Feenders, C.; 916 Mangelsdorf, K.; Harder, J.; Steinbüchel, A.; Blasius, B.; Reinhardt, R.; 917 Rabus, R. Physiological and Proteomic Adaptation of “Aromatoleum 918 Aromaticum” EbN1 to Low Growth Rates in Benzoate-Limited, 919 Anoxic Chemostats. *J. Bacteriol.* **2012**, *194*, 2165–2180.
- 920 (19) Melander, L. C. S.; Saunders, W. H. *Reaction Rates of Isotopic* 921 *Molecules*; John Wiley & Sons, 1980.
- 922 (20) Meyer, A. H.; Penning, H.; Elsner, M. C and N Isotope 923 Fractionation Suggests Similar Mechanisms of Microbial Atrazine 924 Transformation despite Involvement of Different Enzymes (AtzA and 925 TrzN). *Environ. Sci. Technol.* **2009**, *43*, 8079–8085.
- 926 (21) Ehrl, B. N.; Gharasoo, M.; Elsner, M. Isotope Fractionation 927 Pinpoints Membrane Permeability as a Barrier to Atrazine 928 Biodegradation in Gram-Negative Polaromonas Sp. Nea-C. *Environ.* 929 *Sci. Technol.* **2018**, *52*, 4137–4144.
- 930 (22) O’Leary, M. H. Carbon Isotopes in Photosynthesis. *Bioscience* 931 **1988**, *38*, 328–336.
- 932 (23) Wilkes, E. B.; Carter, S. J.; Pearson, A. CO₂-Dependent Carbon 933 Isotope Fractionation in the Dinoflagellate *Alexandrium Tamarense*. 934 *Geochim. Cosmochim. Acta* **2017**, *212*, 48–61.
- 935 (24) Laws, E. A.; Popp, B. N.; Bidigare, R. R.; Kennicutt, M. C.; 936 Macko, S. A. Dependence of Phytoplankton Carbon Isotopic 937 Composition on Growth Rate and [CO₂] Aq: Theoretical 938 Considerations and Experimental Results. *Geochim. Cosmochim. Acta* 939 **1995**, *59*, 1131–1138.
- 940 (25) Aeppli, C.; Berg, M.; Cirpka, O. A.; Holliger, C.; 941 Schwarzenbach, R. P.; Hofstetter, T. B. Influence of Mass-Transfer 942 Limitations on Carbon Isotope Fractionation during Microbial 943 Dechlorination of Trichloroethene. *Environ. Sci. Technol.* **2009**, *43*, 944 8813–8820.
- 945 (26) Vonberg, D.; Vanderborght, J.; Cremer, N.; Pütz, T.; Herbst, 946 M.; Vereecken, H. 20 Years of Long-Term Atrazine Monitoring in a 947 Shallow Aquifer in Western Germany. *Water Res.* **2014**, *50*, 294–306.
- 948 (27) Kundu, K.; Marozava, S.; Ehrl, B.; Merl-Pham, J.; Griebler, C.; 949 Elsner, M. Defining Lower Limits of Biodegradation: Atrazine 950 Degradation Regulated by Mass Transfer and Maintenance Demand 951 in *Arthrobacter Aurescens* TCl. *ISME J.* **2019**, *13*, 2236–2251.
- (28) Ehrl, B. N.; Kundu, K.; Gharasoo, M.; Marozava, S.; Elsner, M. 952 Rate-Limiting Mass Transfer in Micropollutant Degradation Revealed 953 by Isotope Fractionation in Chemostat. *Environ. Sci. Technol.* **2019**, 954 *53*, 1197–1205. 955
- (29) Marozava, S.; Röling, W. F. M.; Seifert, J.; Küffner, R.; Von 956 Bergen, M.; Meckenstock, R. U. Physiology of *Geobacter Metal-* 957 *lireducens* under Excess and Limitation of Electron Donors. Part II. 958 Mimicking Environmental Conditions during Cultivation in Retento- 959 stats. *Syst. Appl. Microbiol.* **2014**, *37*, 287–295. 960
- (30) Trautwein, K.; Grundmann, O.; Wöhlbrand, L.; Eberlein, C.; 961 Boll, M.; Rabus, R. Benzoate Mediates Repression of C₄- 962 Dicarboxylate Utilization in “*Aromatoleum Aromaticum*” EbN1. *J.* 963 *Bacteriol.* **2012**, *194*, 518–528. 964
- (31) Edwards, V. H. The Influence of High Substrate Concen- 965 trations on Microbial Kinetics. *Biotechnol. Bioeng.* **1970**, *12*, 679–712. 966
- (32) Haldane, J. B. S. *Enzymes*; MIT Press: Cambridge, 1965. 967
- (33) Hao, O. J.; Kim, M. H.; Seagren, E. A.; Kim, H. Kinetics of 968 Phenol and Chlorophenol Utilization by *Acinetobacter* Species. 969 *Chemosphere* **2002**, *46*, 797–807. 970
- (34) DiMarco, A. A.; Averhoff, B.; Ornston, L. N. Identification of 971 the Transcriptional Activator PobR and Characterization of Its Role 972 in the Expression of PobA, the Structural Gene for p-Hydrox- 973 ybenzoate Hydroxylase in *Acinetobacter Calcoaceticus*. *J. Bacteriol.* 974 **1993**, *175*, 4499–4506. 975
- (35) Egli, T. The Ecological and Physiological Significance of the 976 Growth of Heterotrophic Microorganisms with Mixtures of 977 Substrates. *Advances in Microbial Ecology*; Springer, 1995; pp 305– 978 386. 979
- (36) Heipieper, H. J.; Meinhardt, F.; Segura, A. The Cis–Trans 980 Isomerase of Unsaturated Fatty Acids in *Pseudomonas* and *Vibrio*: 981 Biochemistry, Molecular Biology and Physiological Function of a 982 Unique Stress Adaptive Mechanism. *FEMS Microbiol. Lett.* **2003**, *229*, 983 1–7. 984
- (37) Unell, M.; Kabelitz, N.; Jansson, J. K.; Heipieper, H. J. 985 Adaptation of the Psychrotroph *Arthrobacter Chlorophenolicus* A6 to 986 Growth Temperature and the Presence of Phenols by Changes in the 987 Anteiso/Iso Ratio of Branched Fatty Acids. *FEMS Microbiol. Lett.* 988 **2007**, *266*, 138–143. 989
- (38) Jensen, J. Chlorophenols in the Terrestrial Environment. 990 *Reviews of Environmental Contamination and Toxicology*; Springer, 991 1996; pp 25–51. 992
- (39) Wild, S.; Harrad, S. J.; Jones, K. C. Chlorophenols in Digested 993 UK Sewage Sludges. *Water Res.* **1993**, *27*, 1527–1534. 994
- (40) Weber, F. J.; de Bont, J. A. M. Adaptation Mechanisms of 995 Microorganisms to the Toxic Effects of Organic Solvents on 996 Membranes. *Biochim. Biophys. Acta, Rev. Biomembr.* **1996**, *1286*, 997 225–245. 998
- (41) Basak, B.; Bhunia, B.; Dutta, S.; Dey, A. Enhanced 999 Biodegradation of 4-Chlorophenol by *Candida Tropicalis* PHB5 via 1000 Optimization of Physicochemical Parameters Using Taguchi 1001 Orthogonal Array Approach. *Int. Biodeterior. Biodegrad.* **2013**, *78*, 1002 17–23. 1003
- (42) Scheublin, T. R.; Deusch, S.; Moreno-Forero, S. K.; Müller, J. 1004 A.; van der Meer, J. R.; Leveau, J. H. J. Transcriptional Profiling of G 1005 Ram-Positive A *Rthrobacter* in the Phyllosphere: Induction of 1006 Pollutant Degradation Genes by Natural Plant Phenolic Compounds. 1007 *Environ. Microbiol.* **2014**, *16*, 2212–2225. 1008
- (43) Nordin, K.; Unell, M.; Jansson, J. K. Novel 4-Chlorophenol 1009 Degradation Gene Cluster and Degradation Route via Hydroxyquinol 1010 in *Arthrobacter Chlorophenolicus* A6. *Appl. Environ. Microbiol.* **2005**, 1011 *71*, 6538–6544. 1012
- (44) Wei, X.; Gilevska, T.; Wetzig, F.; Dorer, C.; Richnow, H.-H.; 1013 Vogt, C. Characterization of Phenol and Cresol Biodegradation by 1014 Compound-Specific Stable Isotope Analysis. *Environ. Pollut.* **2016**, 1015 *210*, 166–173. 1016
- (45) Wunderlich, A.; Heipieper, H. J.; Elsner, M.; Einsiedl, F. 1017 Solvent Stress-Induced Changes in Membrane Fatty Acid Composi- 1018 tion of Denitrifying Bacteria Reduce the Extent of Nitrogen Stable 1019

- 1020 Isotope Fractionation during Denitrification. *Geochim. Cosmochim. Acta* **2018**, *239*, 275–283.
- 1022 (46) Props, R.; Monsieure, P.; Vandamme, P.; Leys, N.; Deneff, V. J.; 1023 Boon, N. Gene Expansion and Positive Selection as Bacterial 1024 Adaptations to Oligotrophic Conditions. *Mosphere* **2019**, *4*, 1025 No. e00011.
- 1026 (47) Pfennig, N.; Wagener, S. An Improved Method of Preparing 1027 Wet Mounts for Photomicrographs of Microorganisms. *J. Microbiol. Methods* **1986**, *4*, 303–306.
- 1028 (48) Hoefs, J.; Hoefs, J. *Stable Isotope Geochemistry*; Springer, 2009; 1029 Vol. 285.
- 1031 (49) Coplen, T. B. Guidelines and Recommended Terms for 1032 Expression of Stable-Isotope-Ratio and Gas-Ratio Measurement 1033 Results. *Rapid Commun. Mass Spectrom.* **2011**, *25*, 2538–2560.
- 1034 (50) Hayes, J. M. Practice and Principles of Isotopic Measurements 1035 in Organic Geochemistry. *Org. Geochem. Contemp. Anc. Sediments* 1036 **1983**, *5*, No. e5.
- 1037 (51) Werner, R. A.; Brand, W. A. Referencing Strategies and 1038 Techniques in Stable Isotope Ratio Analysis. *Rapid Commun. Mass Spectrom.* **2001**, *15*, 501–519.
- 1040 (52) Sherlock. Microbial Identification System, *MIS Operating 1041 Manual*, 2012, pp 2.7–2.18.
- 1042 (53) Wisniewski, J. R.; Zougman, A.; Nagaraj, N.; Mann, M. 1043 Universal Sample Preparation Method for Proteome Analysis. *Nat. Methods* **2009**, *6*, 359–362.
- 1045 (54) Ritchie, M. E.; Phipson, B.; Wu, D.; Hu, Y.; Law, C. W.; Shi, 1046 W.; Smyth, G. K. Limma Powers Differential Expression Analyses for 1047 RNA-Sequencing and Microarray Studies. *Nucleic Acids Res.* **2015**, *43*, 1048 No. e47.
- 1049 (55) Law, C. W.; Chen, Y.; Shi, W.; Smyth, G. K. Voom: Precision 1050 Weights Unlock Linear Model Analysis Tools for RNA-Seq Read 1051 Counts. *Genome Biol.* **2014**, *15*, R29.
- 1052 (56) Smyth, G. K. Linear Models and Empirical Bayes Methods for 1053 Assessing Differential Expression in Microarray Experiments. *Stat. Appl. Genet. Mol. Biol.* **2004**, *3*, 1–25.
- 1055 (57) Benjamini, Y.; Hochberg, Y. Controlling the False Discovery 1056 Rate: A Practical and Powerful Approach to Multiple Testing. *J. R. Stat. Soc., Ser. B* **1995**, *57*, 289–300.
- 1058 (58) Waskom, M.; Botvinnik, O.; O’Kane, D.; Hobson, P.; David, Y. 1059 H.; Lukauskas, S.; Cole, J. B.; Warmenhoven, J.; de Ruiter, J.; Hoyer, 1060 S.; et al. *Seaborn*: V0. 9.0; Zenodo, 2018; Vol. 10.
- 1061 (59) Reed, M. C.; Lieb, A.; Nijhout, H. F. The Biological 1062 Significance of Substrate Inhibition: A Mechanism with Diverse 1063 Functions. *Bioessays* **2010**, *32*, 422–429.
- 1064 (60) Bakhshi, Z.; Najafpour, G.; Kariminezhad, E.; Pishgar, R.; 1065 Mousavi, N.; Taghizade, T. Growth Kinetic Models for Phenol 1066 Biodegradation in a Batch Culture of *Pseudomonas Putida*. *Environ. Technol.* **2011**, *32*, 1835–1841.
- 1068 (61) Erekat, S. I.; Abdelkader, A. A.; Nasereddin, A. F.; Al-Jawabreh, 1069 A. O.; Zaid, T. M.; Letnik, I.; Abdeen, Z. A. Isolation and 1070 Characterization of Phenol Degrading Bacterium Strain *Bacillus Thuringiensis* J20 from Olive Waste in Palestine. *J. Environ. Sci. Health, Part A: Toxic/Hazard. Subst. Environ. Eng.* **2018**, *53*, 39–45.
- 1073 (62) Wijker, R. S.; Zeyer, J.; Hofstetter, T. B. Isotope Fractionation 1074 Associated with the Simultaneous Biodegradation of Multiple 1075 Nitrophenol Isomers by *Pseudomonas Putida* B2. *Environ. Sci.: Processes Impacts* **2017**, *19*, 775–784.
- 1077 (63) Bernstein, A.; Golan, R.; Gelman, F.; Kuder, T. Microbial 1078 Oxidation of Tri-Halogenated Phenols-Multi-Element Isotope 1079 Fractionation. *Int. Biodeterior. Biodegrad.* **2019**, *145*, 104811.
- 1080 (64) Wijker, R. S.; Pati, S. G.; Zeyer, J.; Hofstetter, T. B. Enzyme 1081 Kinetics of Different Types of Flavin-Dependent Monooxygenases 1082 Determine the Observable Contaminant Stable Isotope Fractionation. 1083 *Environ. Sci. Technol. Lett.* **2015**, *2*, 329–334.
- 1084 (65) Elsner, M.; Zwank, L.; Hunkeler, D.; Schwarzenbach, R. P. A 1085 New Concept Linking Observable Stable Isotope Fractionation to 1086 Transformation Pathways of Organic Pollutants. *Environ. Sci. Technol.* 1087 **2005**, *39*, 6896–6916.
- (66) Kaneda, T. Iso-and Anteiso-Fatty Acids in Bacteria: Biosyn- 1088 thesis, Function, and Taxonomic Significance. *Microbiol. Mol. Biol. Rev.* **1991**, *55*, 288–302. 1089
- (67) Sinensky, M. Homeoviscous Adaptation—a Homeostatic 1091 Process That Regulates the Viscosity of Membrane Lipids in 1092 *Escherichia Coli*. *Proc. Natl. Acad. Sci. U.S.A.* **1974**, *71*, 522–525. 1093
- (68) Marozava, S.; Vargas-López, R.; Tian, Y.; Merl-Pham, J.; 1094 Braster, M.; Meckenstock, R. U.; Smidt, H.; Röling, W. F. M.; 1095 Westerhoff, H. V. Metabolic Flexibility of a Prospective Bioremedia- 1096 tor: *Desulfotobacterium Hafniense* Y51 Challenged in Chemostats. 1097 *Environ. Microbiol.* **2018**, *20*, 2652–2669. 1098
- (69) Tatusov, R. L.; Galperin, M. Y.; Natale, D. A.; Koonin, E. V. 1099 The COG Database: A Tool for Genome-Scale Analysis of Protein 1100 Functions and Evolution. *Nucleic Acids Res.* **2000**, *28*, 33–36. 1101
- (70) Arora, P.; Bae, H. Bacterial Degradation of Chlorophenols and 1102 Their Derivatives. *Microb. Cell Fact.* **2014**, *13*, 31. 1103
- (71) Kang, C.; Yang, J. W.; Cho, W.; Kwak, S.; Park, S.; Lim, Y.; 1104 Choe, J. W.; Kim, H. S. Oxidative Biodegradation of 4-Chlorophenol 1105 by Using Recombinant Monooxygenase Cloned and Overexpressed 1106 from *Arthrobacter Chlorophenicus* A6. *Bioresour. Technol.* **2017**, 1107 *240*, 123–129. 1108
- (72) Cho, S. Y.; Kwean, O. S.; Yang, J. W.; Cho, W.; Kwak, S.; Park, 1109 S.; Lim, Y.; Kim, H. S. Identification of the Upstream 4-Chlorophenol 1110 Biodegradation Pathway Using a Recombinant Monooxygenase from 1111 *Arthrobacter Chlorophenicus* A6. *Bioresour. Technol.* **2017**, *245*, 1112 1800–1807. 1113
- (73) Pati, S. G.; Kohler, H.-P. E.; Pabis, A.; Paneth, P.; Parales, R. E.; 1114 Hofstetter, T. B. Substrate and Enzyme Specificity of the Kinetic 1115 Isotope Effects Associated with the Dioxygenation of Nitroaromatic 1116 Contaminants. *Environ. Sci. Technol.* **2016**, *50*, 6708–6716. 1117
- (74) Dorer, C.; Vogt, C.; Kleinstaub, S.; Stams, A. J. M.; Richnow, 1118 H.-H. Compound-Specific Isotope Analysis as a Tool to Characterize 1119 Biodegradation of Ethylbenzene. *Environ. Sci. Technol.* **2014**, *48*, 1120 9122–9132. 1121
- (75) Sun, F.; Mellage, A.; Gharasoo, M.; Melsbach, A.; Cao, X.; 1122 Zimmermann, R.; Griebler, C.; Thullner, M.; Cirpka, O. A.; Elsner, 1123 M. Mass-Transfer-Limited Biodegradation at Low Concentrations— 1124 Evidence from Reactive Transport Modeling of Isotope Profiles in a 1125 Bench-Scale Aquifer. *Environ. Sci. Technol.* **2021**, *55*, 7385. 1126
- (76) Tjihuis, L.; Van Loosdrecht, M. C. M.; Heijnen, J. J. A 1127 Thermodynamically Based Correlation for Maintenance Gibbs Energy 1128 Requirements in Aerobic and Anaerobic Chemotrophic Growth. 1129 *Biotechnol. Bioeng.* **1993**, *42*, 509–519. 1130
- (77) Suma, Y.; Lim, H.; Kwean, O. S.; Cho, S.; Yang, J.; Kim, Y.; 1131 Kang, C. S.; Kim, H. S. Enzymatic Degradation of Aromatic 1132 Hydrocarbon Intermediates Using a Recombinant Dioxygenase 1133 Immobilized onto Surfactant-Activated Carbon Nanotube. *Bioresour. Technol.* **2016**, *210*, 117–122. 1134 1135